Environmental Science & Technology

ARTICLE

pubs.acs.org/est

Physicochemical and Toxicological Properties of Commercial Carbon Blacks Modified by Reaction with Ozone

Brian C. Peebles,[†] Prabir K. Dutta,[*,†] W. James Waldman,[‡] Frederick A. Villamena,[§] Kevin Nash,[§] Michael Severance,[†] and Amber Nagy[‡]

[†]Department of Chemistry, The Ohio State University, 100 West 18th Avenue, Columbus, Ohio 43210, United States

[‡]Department of Pathology, The Ohio State University, 4160 Graves Hall, 333 West 10th Avenue, Columbus, Ohio 43210, United States

[§]Department of Pharmacology, The Ohio State University, 390 Biomedical Research Tower, 460 West 12th Avenue, Columbus, Ohio 43210, United States

Supporting Information

ABSTRACT: Ozonation of two commercial carbon blacks (CBs), Printex 90 (P90) and Flammruss 101 (F101), was carried out and changes in their morphology, physical properties, and cytotoxicity were examined. The hypothesis examined was that different methods of manufacture of CBs influence their chemical reactivity and toxicological properties. Structural changes were examined by X-ray photoelectron spectroscopy, infrared spectroscopy, Raman spectroscopy, and electron paramagnetic resonance spectroscopy (EPR). Introduction of surface oxygen functionality upon ozonation led to changes in surface charge, aggregation characteristics, and free radical content of the CBs. However, these changes in surface functionality did not alter the cytotoxicity and release of inflammation markers upon exposure of the CBs to murine macrophages. Interaction of macrophages with F101 resulted in higher levels of inflammatory markers than P90, and the only structural correlation was with the higher persistent radical concentration on the F101.

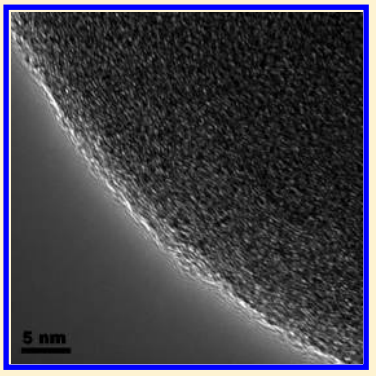

INTRODUCTION

Carbon black (CB) is the product of incomplete combustion of hydrocarbon feedstock and is an important technological material. It is used as a pigment in paints, inks, and toners, a reinforcing agent in rubber and polymers, a conductivity enhancer in polymers, an adsorbent, and a support for catalysts. The many industrial uses of CB and carbonaceous materials make it necessary to tailor their physical and chemical properties. Surface functionalization of CB is an active area of research; in particular, using ozone to introduce oxygen functionalities.[1−7]

Carbon black is also chemically similar to the carbonaceous component of environmentally relevant particles such as soot and coal fly ash.[2,8] There is considerable research activity in the use of nanoparticles in biological systems,[9] and the physiological effects of CBs, particularly their toxic and inflammatory response, are of interest.[10,11]

In this study, two commercial CBs, Flammruss 101, a lamp black (F101, prepared by burning liquids with a restricted air supply and quenched by deposition on a cool surface), and Printex 90, a furnace black (P90, made by partial combustion of residual aromatic oils, and quenched by water) were examined. The hypothesis behind this study is that methods of manufacture of CBs determine their chemical reactivity, as evidenced by oxidative functionalization and toxicology properties, as measured by interaction of the CBs with murine macrophages. Because of their technological relevance, there have been numerous studies on toxicity and effects of workplace exposure to CBs. Of particular interest is the report of a lack of lung tumor formation in mice upon inhalation exposure to P90, as compared to controls.[12] For intratracheally administered F101 and P90 in rats, the tumor incidence was higher in rats exposed to P90 at 21% (10 out of 48 rats) compared to 8% (4 out of 48 rats) exposed to F101.[13] In this study, we report that the evolution of surface oxygen functionality upon ozonation influences surface charge, morphology, size, and toxicity. The cytotoxicity and inflammatory properties of CBs and correlations with the surface chemistry are also relevant to occupational and environmental exposure.

EXPERIMENTAL SECTION

Physicochemical Characterization. F101 and P90 CB particles (from Degussa) were characterized as obtained, and after ozonolysis. Ozonolysis of F101 and P90 was performed over a 4-h period using an Enaly EOZ-300Y corona discharge ozone generator (Ozone Solutions, Hull, Iowa) that produces approximately 40 mg of ozone per hour in a stream of 20% oxygen. The generator was supplied with a flow of approximately 100 mL/minute compressed air that had been passed through a hydrocarbon trap and a desiccant. The ozone generator was connected to the tip of a buret, which was loaded with 500 mg of CB (fluid bed geometry).

Received: March 17, 2011
Accepted: November 4, 2011
Revised: October 31, 2011
Published: November 04, 2011

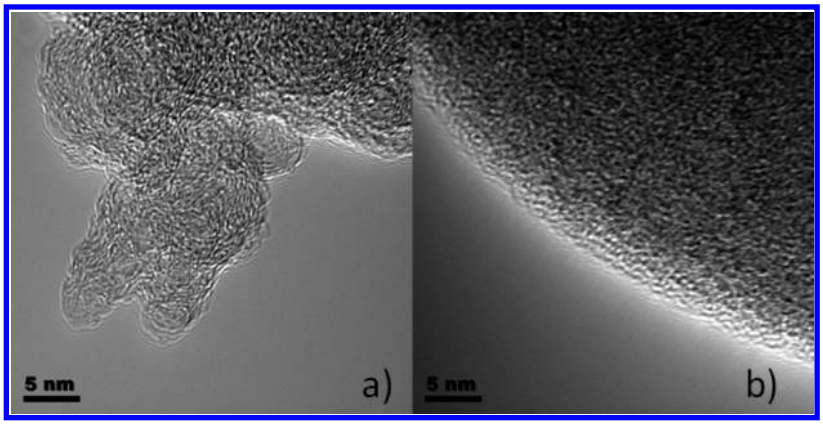

Figure 1. TEM images of (a) untreated P90 and (b) untreated F101.

X-ray photoelectron spectroscopy was performed using a Kratos Ultra Axis spectrometer with a monochromatic Al Kα source. Spectral analysis was performed using CasaXPS software. Ultraviolet photoelectron spectroscopy was performed using a He (I) ultraviolet light source with a helium pressure of $\sim 5 \times 10^{-8}$ Torr. The EPR spectrometer (Bruker EMX X-band) was operated at the X-band (9.87 GHz) with 10 mW microwave power, 1 G modulation amplitude, receiver gain of 1.0×10^5, 21.5 s scan time, and 42 s time constant with a 120 G sweep width.

A Perkin-Elmer Spectrum 400 FTIR spectrometer was fitted with a Pike Technologies 100-mm gas cell with calcium fluoride windows. The carbon samples were coated on the IR window and exposed to ozone. Baseline-corrected spectra were translated to zero at 2000 cm^{-1}, a point at which all of the spectra had approximately the same slope and no spectral features. Powders were pressed onto the surfaces of Teflon discs and placed on the stage of a Renishaw InVia Raman microprobe equipped with a 633 nm He−Ne laser. Particles were imaged by transmission electron microscopy using a Tecnai F20 transmission electron microscope. Dynamic light scattering (DLS) and zeta potential measurements were made using a Malvern ZetaSizer Nano instrument (sample loading 10 mg/L, 30 s sonication prior to use).

Macrophage Toxicity Studies. The murine alveolar macrophage cell line (MH-S) was purchased from the American Type Culture Collection (Manassas, VA), and propagated as described previously.[14] Cells were plated in 24 well plates at a density of 1×10^5 cells/well. Carbon blacks were suspended in PBS, sonicated for 30 s and added to confluent murine macrophage monolayers at a concentration ranging from 2.5 to 10 $\mu g/cm^2$. Cells treated with 1% Triton-100 (Sigma) served as a positive control for lactate dehydrogenase (LDH) release assays, while cells treated with *E. coli* lipopolysaccharide (LPS, Sigma) served as the positive control for tumor necrosis factor-alpha (TNF-α) ELISAs. Supernatants were collected from each well and clarified by centrifugation at 16 000 RCF for 2 min to pellet uninternalized carbon nanoparticles. Lactate dehydrogenase and TNF-α secretion was measured via ELISA assays as described previously.[14] ELISA assays for IL-1β were also carried out according to manufacturer's instructions (R&D Systems, Minneapolis, MN). There was no interference of CB on the assays, and these results are shown in Supporting Information.

RESULTS

Characterization of CB and Its Reaction with Ozone. *Morphology.* Transmission electron microscope images of the two carbon samples are shown in Figure 1. Flammruss 101 comprises well-defined primary particles that have an average diameter of ~100 nm, with little surface "roughness", whereas P90 has more "roughness" on its surface. These micrographs are consistent with the Heckman and Harling model of CB structure.[15] The morphologies of P90 and F101 were not noticeably changed after 4 h of ozone exposure (Figure S1, Supporting Information). The surface areas of P90 and F101 measured by BET were 320 and 33 m^2/g, respectively. Upon ozonation for 4 h, the surface areas changed to 316 and 44 m^2/g for P90 and F101, respectively.

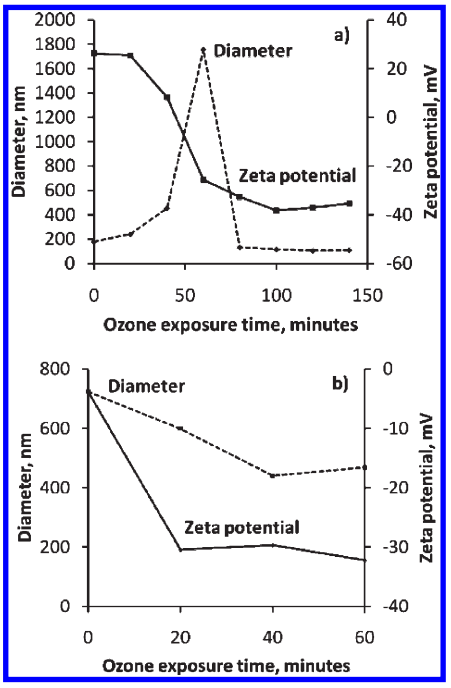

Figure 2. Changes in particle diameter (dashed) and zeta potential (solid) for (a) P90 and (b) F101 upon exposure to ozone (particles dispersed in water).

Size and Surface Charge. Figure 2a shows that the average hydrodynamic diameter of untreated Printex 90 was ~180 ± 0.7 nm in water at pH 5, with an average zeta potential of ~26.3 ± 1.9 mV. The positive zeta potential reflects a basic carbon black surface.[16] This basicity is also reflected as an increase in the pH of ultrapure water from pH 6.7 to 7.1 with suspended P90 (50 mg/mL). For F101 (Figure 2b), the initial

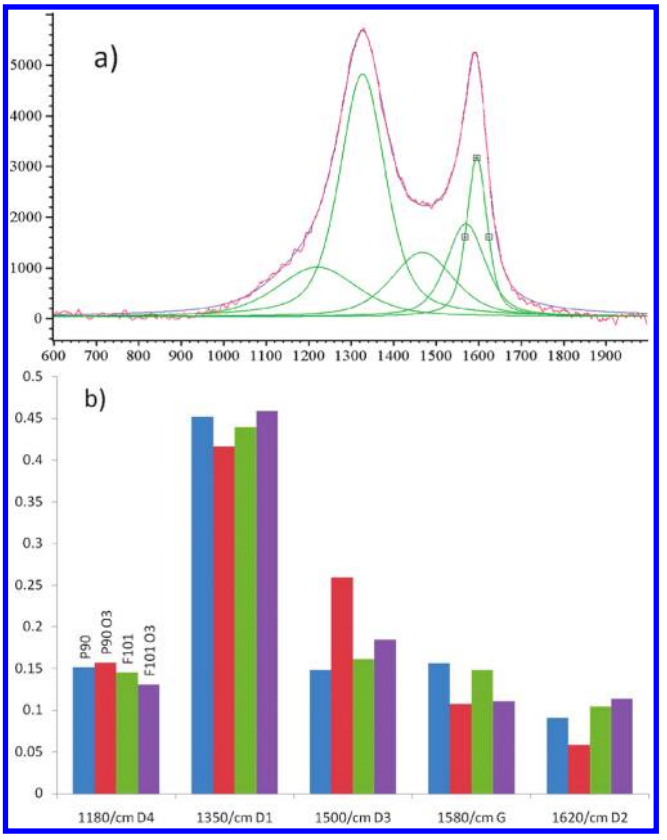

Figure 3. (a) Raman spectrum of P90 after ozonolysis, showing bands characteristic of commercial carbon blacks. (b) Relative area comparison of Raman bands of ozonated and untreated P90 and F101.

size in water was ~724 ± 71 nm and the zeta potential was negative at ~ −4 ± 1.2 mV. This is indicative of an acidic surface,[16] and reflected in the decrease in pH from 6.7 to 4.2 when 50 mg/mL F101 was added to ultrapure water. These samples were highly polydisperse (polydispersity index PDI ranging from 0.2 for P90 to 0.5 for F101). Though TEM indicates primary sizes of both the CB were <100 nm, the CBs are significantly agglomerated.

Upon exposure to ozone, dramatic changes were observed in the surface charge and size. With increasing exposure to ozone, the zeta potential of P90 became less positive, and the agglomerate size increased and reached a peak of 1.8 ± 0.43 μm in the 40−80 min exposure time. With further ozonation, the size decreased to ~110 ± 3.5 nm and the zeta potential reached ~ −35.3 ± 1.6 mV. Upon ozonation of F101 (Figure 2b), the zeta potential fell from ~ −4 to ~ −30.5 ± 0.4 mV in the first 20 min and the average agglomerate diameter decreased from ~724 to ~598 ± 112 nm. The zeta potential remained nearly constant upon further ozone treatment as the average diameter of the particle agglomerates stabilized to ~468 ± 40 nm. The ozonated F101 samples were highly polydisperse with PDI ranging from 0.4 to 0.6, whereas for ozonated P90, the PDIs ranged from 0.1 to 0.3, except for the highly agglomerated sample at 60 min, which had a PDI of 0.9 (indicating a very broad particle distribution).

Raman Spectroscopy. Raman spectra of P90 and F101 were generally similar, with the spectrum for ozonated P90 shown in Figure 3a. The most prominent features of the spectrum are bands at ~1350 and 1580 cm^{-1}, the "D1" band and "G" band, respectively. Three other bands used for curve fitting are at 1180 (D4), 1500 (D3), and 1620 (D2) cm^{-1}. Raman spectra of CBs have been investigated in detail and there is agreement in band assignments.[8,17,18] Disorder or defect (D) bands are at 1620 cm^{-1} (D2), assigned to surface graphene disorder, the 1500 cm^{-1} (D3) band assigned to carbon with functional groups, 1350 cm^{-1} (D1) band assigned to graphene layer edges, and the 1180 cm^{-1} (D4) band assigned to C=C vibrations of polyene-like structures. The band at 1580 cm^{-1} (G) arises from the ideal graphitic lattice vibration. Figure 3b plots the relative intensities of these five bands for P90 and F101 before and after treatment with ozone. More marked changes were observed for P90, with significant increase in D3 due to formation of surface functional groups, at the expense of graphene bands (G and D2).

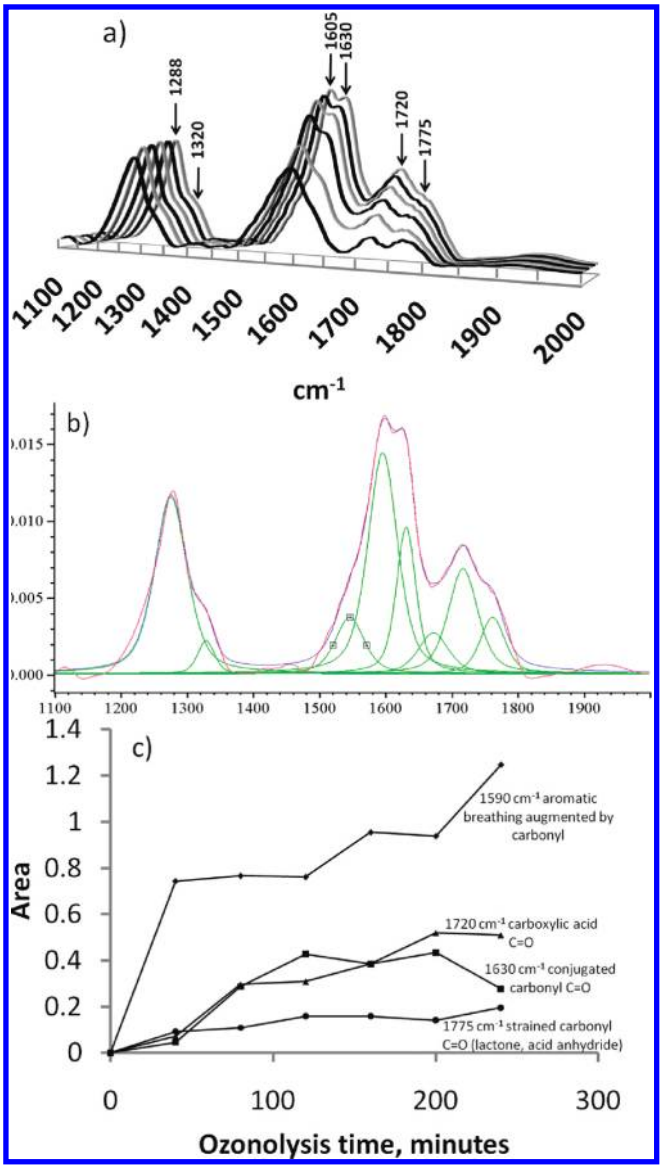

Figure 4. (a) Difference spectra of P90 exposed to ozone, taken at 40-min intervals, starting at 40 min (front) and finishing at 240 min (back). (b) Curve fitting of the infrared difference spectrum of P90 exposed to ozone for 240 min. (c) Plot of the areas of integrated bands of P90 difference spectra vs ozonolysis time.

Infrared Spectroscopy. The infrared spectra of P90 and F101 were similar. There are three bands: a weak band at ~1730 cm^{-1}, and sharper bands at ~1590 and ~1240 cm^{-1}. The band around

1730 cm^{-1} is assigned to a mix of carbonyl functionalities, and the band at 1590 cm^{-1} corresponds to aromatic ring stretching.[19,20] The band at 1240 cm^{-1} can arise from lactones, ethers, and the symmetric bend of hydrogen atoms on adjacent double-bonded carbon atoms.[5,21]

To evaluate the changes taking place during ozonation, difference spectra of P90 and F101 were obtained between the ozonated samples and the starting material. The data for P90 is shown in Figure 4. Data for F101 is shown after 240 min of ozonolysis in Figure S2, and the evolution of bands as a function of reaction time with ozone is shown for P90 in Figure 4a. The changes from ozonation were more marked in P90 as compared to F101 (the band at 1600−1650 cm^{-1} is five times as intense in P90 as compared to F101), and could be readily followed upon ozonation.

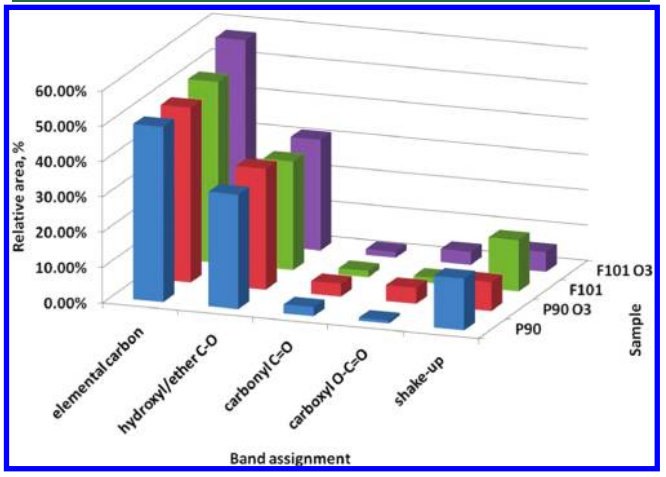

Figure 5. Relative area of C 1s XPS peaks before and after ozonolysis.

The spectra were deconvoluted into 8 bands as shown in Figure 4b. The major bands are at 1775, 1720, 1630, 1605, 1320, and 1288 cm^{-1}. The band at 1775 cm^{-1} has been assigned to carbonyl groups on strained functionality like lactones and acid anhydrides.[19,22,23] The band centered at ∼1720 cm^{-1} has been assigned to carboxylic acids.[19,22] The bands at 1630 and 1605 cm^{-1} represent conjugated carbonyls and the carbon backbone, respectively, with the band at 1600 cm^{-1} being enhanced by the carboxyl group. Intensity in the ∼1600 cm^{-1} region can also arise from C═O vibrations conjugated with large ring structures (>25). Vicinal −OH groups are also reported to promote intensity of this band.[19,22] Bands formed at 1320 and 1288 cm^{-1} were assigned to C−O single bonds in strained and unstrained cyclic ethers, respectively.[19,20] Figure 4c is a plot of the intensity of the four major bands as a function of ozonation time. The 1630 and 1720 cm^{-1} bands increase with similar slopes, which might be expected since they are related. The strained carbonyl groups at 1775 cm^{-1} appear rapidly but then saturate, indicating that the sites at which initial carbonylation takes place are the most reactive.

Surface Spectroscopy. X-ray photoelectron spectra (XPS) in the C 1s region were similar for P90 and F101. The changes upon ozonation for P90 are shown in Figure S3. The O 1s shows a broad peak at 532.5 eV (shown in the left inset in Figure S3). The C 1s region was deconvoluted into five peaks. They represent C−C and C−H bonded carbon, C−O and ether carbon, carbonyl carbon, carboxyl carbon, and a $\pi \rightarrow \pi^*$ shakeup satellite,[1,24,25] with binding energies of ∼284.8, 285.4, 287.5, 288.9, and 291.0 eV, respectively (seen clearly in the inset for the last four peaks in Figure S3). The $\pi \rightarrow \pi^*$ shakeup satellite peak arises from the interaction of the excited C1s electron with the π electrons of the aromatic structure. The quantitative distribution of the various functionalities is shown in Figure 5 for P90 and F101, before and after ozonation. Upon reaction with ozone, there was an increase in C═O functionalities at

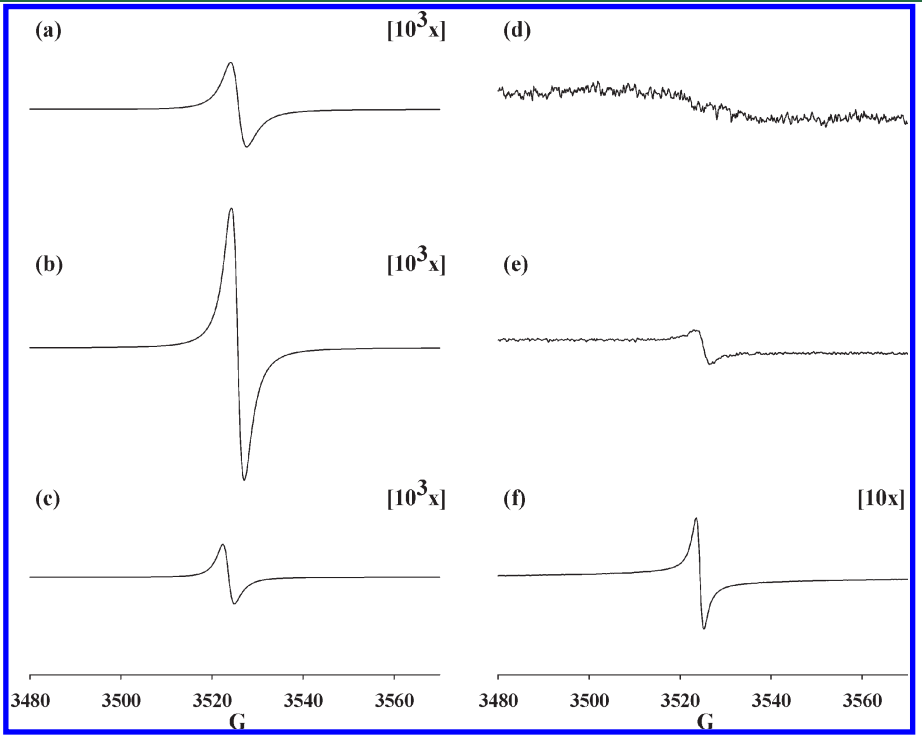

Figure 6. X-Band spectra of untreated solid (a) F101and (d) P90, ozonated solid (b) F101and (e) P90, and ozonated samples exposed to PBS buffer (c) F101and (f) P90.

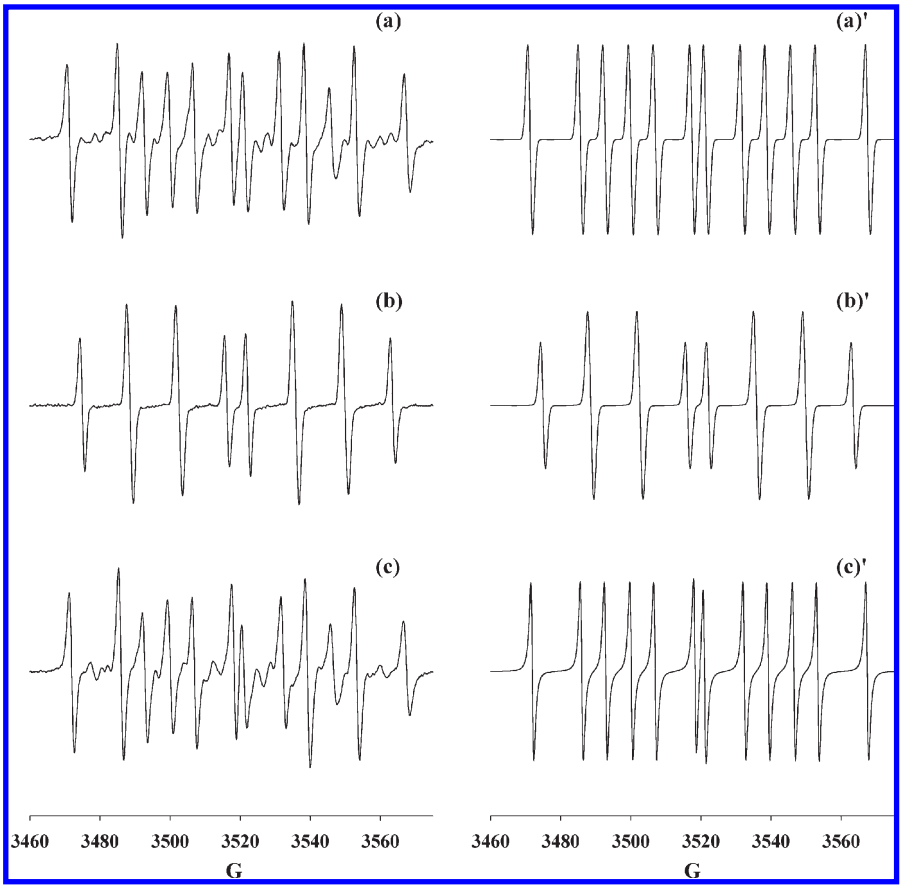

Figure 7. X-band spectra of (a) carbon-centered adduct of DEPMPO generated from ozonated aqueous F101 (DEPMPO−R, 95%, a_N = 14.4, a_H = 21.4, a_P = 46.1, g = 2.0056); (b) hydroxyl adduct of DEPMPO generated from ozonated aqueous P90 (DEPMPO−OH, a_N = 14.0, a_H = 13.2, a_P = 47.2, g = 2.0056); (c) α-hydroxy ethyl adduct of DEPMPO generated from ozonated aqueous P90 in ethanol (DEPMPO−R, 98%, a_N = 14.1, a_H = 20.9, a_P = 46.4, g = 2.0056). (a)′, (b)′, and (c)′ are the corresponding simulations from which the hyperfine constants were obtained.

the expense of the $\pi \rightarrow \pi^*$ shakeup peak, indicating that the graphitic surface was getting oxidized. The oxygenation of the surface was also reflected in the 9-fold O:C ratio increase for P90 and 5.7-fold increase for F101. The decrease in graphitic character upon ozonation was also reflected in the ultraviolet photoelectron spectra (UPS). Figure S4 shows the UPS data with a shoulder on the C 2p band at ∼3 eV attributable to p−π character, which disappeared on ozonation.

EPR Spectroscopy. The EPR spectra of P90 and F101 as-obtained and after treatment with ozone are shown in Figure 6 (raw data are shown in Table S1, Supporting Information). Stable free radicals were detected on F101 with spin content of $2.8 \pm 0.8 \times 10^8$ spins/mg (Figure 6a), whereas for P90, the signal was very weak ($<2.2 \pm 0.8 \times 10^3$ spins/mg) (Figure 6d). Upon ozonation, in both CBs, the free radical content increased, for F101 to $5.8 \pm 0.6 \times 10^8$ spins/mg (Figure 6b), and for P90 to $4.4 \pm 0.9 \times 10^4$ spins/mg (Figure 6e). In the case of ozonated F101, the EPR signal of the solid decreased upon exposure to PBS buffer to $1.1 \pm 0.1 \times 10^8$ spins/mg (Figure 6c), whereas in P90, the signal increased to $1.7 \pm 0.1 \times 10^6$ spins/mg (Figure 6f). The g values in all cases were in the range of 2.0022−2.0028, typical of graphitic compounds.[19] To examine whether the freshly ozonated CB samples release soluble radicals upon contact with PBS buffer, spin trapping experiments were carried out, using DEPMPO as the spin trap.[26,27] As shown in Figure 7, there is a difference in the spin pattern for the radicals observed in solution between the ozonated F101 and P90. In the case of F101, the data is best simulated by a C-centered radical adduct (a_N = 14.4, a_H = 21.4, a_P = 46.1, g = 2.0056) and for P90 an O-centered radical adduct (a_N = 14.0, a_H = 13.2, a_P = 47.2, g = 2.0056). Upon addition of ethanol to P90, the DEPMPO spin pattern suggests the formation of α-hydroxyethylradical (C−centered: a_N = 14.1, a_H = 20.9, a_P = 46.4, g = 2.0056), indicating that ·OH radicals are being formed upon exposure of ozonated P90 to water. Figure S5 shows that the as-obtained CBs also generate radicals upon contact with PBS, but 15−30 fold less than the ozonated samples (P90: 0.22 μM/mg, ozonated P90: 6.1 μM/mg; F101: 0.62 μM/mg, ozonated F101: 10.9 μM/mg, procedure described in Supporting Information along with Figure S6).

Biological Activity of CB. Optical microscopy shows the ready uptake of CBs in the macrophages (a typical micrograph with F101 and P90 is shown in Figure S7). In the RPMI + FBS media used in these assays, the zeta potentials for ozonated P90 and F101 were -11.3 ± 0.2 and -12.6 ± 0.5 mV, with sizes of 218 ± 4 and 554 ± 9 nm, respectively. For the nonozonated P90 and F101 in media, zeta potentials were -11.2 ± 0.4 and -11.5 ± 0.2 mV and sizes were 262 ± 5 and 511 ± 9 nm, respectively (Figure S8 shows a characteristic light scattering and zeta potential data for F101 in media). Protein adsorption from the media is bringing about significant change in the surface charge, especially for P90, which in the as-obtained form in water exhibited a positive charge. Similar changes in charge were reported for a series

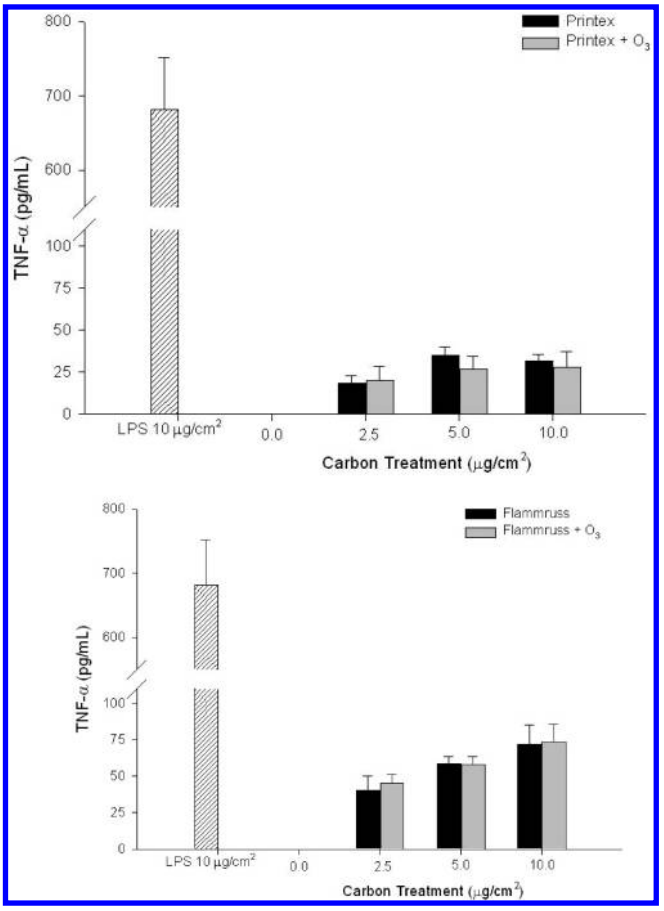

Figure 8. TNF-α assays for macrophages given the same treatment with P90 (top) and F101 (bottom) with and without ozonation (LPS serves as positive control).

of oxide nanoparticles suspended in cell culture media, all of which exhibited comparable negative zeta potentials.[28] Cytotoxicity of the CBs toward macrophages was measured with the lactate dehydrogenase assay. The results are shown in Figure S9. The assay indicated that untreated and ozonated samples of Printex 90 and Flammruss 101 were only slightly cytotoxic. At exposures of 2.5−10 μg F101 or P90 per cm^2 plate area, with or without treatment of particles with ozone, cell death was less than 10%. Upon interaction with macrophages, Printex 90 caused a release of 20−40 pg of the inflammatory cytokine TNF-α per mL of cell media, and F101 resulted in the release of 40−70 pg TNF-α per mL, as shown in Figure 8. For comparison, levels of TNF-α produced by cells in response to stimulation with LPS were 680 pg per mL. Ozone treatment of the CBs had minimal influence on the inflammatory response of exposed cells, as measured by production of TNF-α. IL-1β production by cells treated with either CB ± ozone was negligible (data not shown). In all cases, the supernatants were examined for the biological assays after the removal of the CB, and Figure S10 demonstrates that, in this procedure, the CB did not interfere with the cytotoxicity assay.

DISCUSSION

Two facts emerge from this study: the enhanced reactivity of P90 to ozone, as indicated by Raman, IR, and XPS, and the stronger inflammatory response to F101 upon exposure to macrophages. These results form the basis of this discussion.

Chemical Reactivity. The Raman data shown in Figure 3b suggest that the graphene layers are the primary reaction sites (decrease of intensity of the bands G and D2), resulting in increase of band D3. The decrease in intensity of the $\pi-\pi^*$ shake up peaks shown by XPS also confirms that the reaction is happening on the graphene layers, and changes in peaks in the C 1s region indicate that the reaction products are primarily oxygen functionalities (Figure 5).

Though both of the CBs have graphene content, the different behavior of P90 must stem from its more reactive graphene structures. The UPS data indicate higher intensity $\pi-\pi^*$ peaks (Figure S4) in P90. Graphene layers are known to have basic properties, and explain the positive zeta potential in as-obtained P90, and graphene has also been proposed as sites for ozone adsorption.[29] TEM and the higher surface area of P90 indicate more disorder and thus possible higher reactivity (Figure 1). Infrared spectroscopy shows that the strained carbonyls on P90 have higher intensity after first 30 min of ozonation as compared to the other carbonyl groups (Figure 4b, c), indicating that the sites responsible for the strained carbonyls are more reactive. Eventually, the production of carboxylic acid groups overtook the production of strained carbonyl species, consistent with previous chemical titration results.[7]

Because the oxygen functionality development upon ozonation takes place at different rates on the P90 surface, it indicates that there is a distribution of adsorption sites.[7,30] The edges of structural units might functionalize more easily than the faces, and may be responsible for the strained carbonyl groups; whereas, the conversion of the faces to carbonyl groups is slower and continues with time (Figure 4c).

Development of the negatively charged functionalities upon ozonation altered the zeta potential to more negative values for F101 and caused some deagglomeration (due to electrostatic repulsion between particles) as seen in Figure 2b. For P90, increase in negatively charged functionality with ozonation balanced the positively charged functionality in the starting material leading to a more neutral particle and increase in hydrodynamic diameter. Eventually, the zeta potential became more negative with ozonation and the particle size decreased (Figure 2a).

In both F101 and P90, there is an increase in free radical concentration upon ozonation, in contrast to studies on soot.[31] As compared to freshly prepared soot (10^{15} spins/mg), the spin concentrations in F101 ($\sim 10^8$) and P90 ($<10^3$) are considerably smaller. With freshly prepared soot, the spin concentration was proposed to decrease upon ozonation because of spin pairing interactions with paramagnetic O_2, and does not appear to be taking place with the CBs. Instead, an increase in free radical content is observed with ozonation of the CBs which is consistent with reaction of ozone with aromatic and olefinic compounds. Both F101 and P90 contain graphene. These functionalities will react with ozone to generate ozonides, leading to the "Criegee" intermediate and possible radical formation.[32,33] Upon reaction with water, both CBs should form hydroxyl radicals. In the case of F101, the ·OH appear to be reacting with the CB surface and releasing C-centered radicals into solution. In the case of P90, only the ·OH radicals are observed. It is unclear as to why there is this difference, both CBs have low levels of adsorbed PAH's, though F101is reported to have slightly higher levels than P90 (F101 < 0.1%, P90 < 0.04%).[13]

Biological Properties. Neither P90 nor F101, in the parent form or in the oxidized form, elicited a strong cytotoxic response from exposed macrophages, with fewer than 10% of the cells

dying. There is, however, an inflammatory response for both parent and oxidized particles. The lack of cytotoxic response and the mild inflammatory response are consistent with previous studies.[11,34] Any dependence of the cytotoxicity or inflammatory response for P90 based on initial surface charge (positive to negative upon ozonation) could not be determined since protein adsorption (from the media) on the CB made the surface charge similar for both ozonated and nonozonated samples. F101 provokes a stronger inflammatory response from macrophages than P90. The only structural correlation we find is the EPR data (Figure 6,7), which shows higher inherent free radical contents in F101 in its native form, upon ozonation, and exposure to water, being at least 2 orders of magnitude higher compared to P90. Persistent free radical content and its influence on toxicity of airborne fine particulates have been noted, with the proposed mechanism being redox cycling of semiquinone radicals.[35,36] Both F101 and P90 in their native form release free radicals upon contact with water and the ozonated samples release an order of magnitude more radicals in solution. The solids also retain free radicals with spin content on F101 > P90. The role of the solution radicals released by the CBs upon contact with water on the biological effects observed here is unclear. It is likely that the radicals formed in solution immediately react with the media, and may not make it into the macrophages. However, the solid samples, on the other hand, will carry the persistent free radicals into the cell, and the higher levels of inflammatory markers in F101 over P90 correlate with the higher spin content of F101.

In conclusion, the method of manufacture has a profound influence on the CB. With the furnace black sample (P90), there is more structural disorder and a more reactive surface. Its method of manufacture involves a water quenching step, which may play a role in its surface properties. The lampblack sample (F101) formed via deposition on a cool surface has more entrapped persistent free radicals, is more ordered and less reactive.

■ ASSOCIATED CONTENT

Supporting Information. Detailed structural and spectroscopic data on the CBs and details of the biological activity. This information is available free of charge via the Internet at http://pubs.acs.org.

■ AUTHOR INFORMATION

Corresponding Author
*Tel.: (614) 292-4532. E-mail: dutta@chemistry.ohio-state.edu.

■ ACKNOWLEDGMENT

We acknowledge funding from the NIOSH Grant R01 OH009141 and USDA/NIFA (2011-67021-30360).

■ REFERENCES

(1) Chen, X.; Farber, M.; Gao, Y.; Kulaots, I.; Suuberg, E. M.; Hurt, R. H. Mechanisms of surfactant adsorption on non-polar, air-oxidized, and ozone-treated carbon surfaces. *Carbon* **2003**, *41*, 1489–1500.

(2) Gao, Y.; Külaots, I; Chen, X.; Aggarwal, L; Mehta, A.; Suuberg, E. M.; Hurt, R. H. Ozonation for the chemical modification of carbon surfaces in fly ash. *Fuel* **2001**, *80*, 765–768.

(3) Cataldo, F. Ozone reaction with carbon nanostructures. 2: The reaction of ozone with milled graphite and different carbon black grades. *J. Nanosci. Nanotechnol.* **2007**, *7*, 1446–1454.

(4) Gómez-Serrano, V.; Álvarez, P. M.; Jaramillo, J.; Beltrán, F. J. Formation of oxygen complexes by ozonation of carbonaceous materials prepared from cherry stones. I. Thermal effects. *Carbon* **2002**, *40*, 513–522.

(5) Mul, G.; Neeft, J. P. A.; Kapteijn, F.; Moulijn, J. A. The formation of carbon surface oxygen complexes by oxygen and ozone. The effect of transition metal oxides. *Carbon* **1998**, *9*, 1269–1276.

(6) Lee, G.; Lee, B.; Kim, J.; Cho, K. Ozone adsorption on graphene: Ab initio study and experimental validation. *J. Phys. Chem. C* **2009**, *113*, 14225–14229.

(7) Valdés, H.; Sánchez-Polo, M.; Rivera-Utrilla, J; Zaror, C. A. Effect of ozone treatment on surface properties of activated carbon. *Langmuir* **2002**, *18*, 2111–2116.

(8) Liu, Y.; Liu, C.; Ma, J.; Ma, Q.; He, H. Structural and hygroscopic changes of soot during heterogeneous reaction with O_3. *Phys. Chem. Chem. Phys.* **2010**, *12*, 10896–10903.

(9) Stark, W. J. Nanoparticles in Biological Systems. *Angew. Chem. Int. Ed.* **2011**, *50*, 1242–1258.

(10) Grassian, V. H., Ed. *Nanoscience and Nanotechnology: Environmental and Health Impacts*; John Wiley & Sons: Hoboken, NJ, 2008.

(11) Donaldson, K.; Born, P. J. A.; Oberdorster, G.; Pinkerton, K. E.; Stone, V.; Tran, C. L. Concordance between *in vitro* and *in vitro* delivery in the proinflammatory effects of low-toxicity, low-solubility particles: the key role of the proximal alveolar region. *Inhalat. Toxicol.* **2008**, *20*, 53–62.

(12) Heinrich, U.; Fuhst, R.; Rittinghausen, R. Chronic inhalation exposure of Wistar rats and two different strains of mice to diesel exhaust, carbon black and titanium dioxide. *Inhalat. Toxicol.* **1995**, *7*, 533–556.

(13) Pott, F.; Roller, M. Carcinogenicity Studies with nineteen granular dusts in rats. *Eur. J. Oncol.* **2005**, *10*, 249–281.

(14) Peebles, B. C.; Dutta, P. K.; Nagy, A.; Waldman, W. J. Fenton activity and cytotoxicity studies of iron-loaded carbon particles. *Environ. Sci. Technol.* **2010**, *44*, 6887–6892.

(15) Donnet, J.-B.; Custodero, E. La microscopie à effet tunnel des poudres, application aux noirs de carbone. *C. R. Acad. Sci., Ser. II* **1992**, *314* (6), 579–584.

(16) Xu, R.; Wu, C.; Xu, H. Particle size and zeta potential of carbon black in liquid media. *Carbon* **2007**, *45*, 2806–2809.

(17) Ferrari, A. C.; Robertson, J. Interpretation of Raman spectra of disordered and amorphous carbon. *Phys. Rev. B* **2000**, *61* (20), 14095–14107.

(18) Sadezky, A.; Muckenhuber, H.; Grothe, H.; Neissner, R.; Pöschl, U. Raman microscopy of soot and related carbonaceous materials: Spectral analysis and spectral information. *Carbon* **2005**, *43*, 1731–1742.

(19) Akhter, M. S.; Chughtai, A. R.; Smith, D. M. The structure of hexane soot I: Spectroscopic studies. *Appl. Spectrosc.* **1985**, *39* (1), 143–153.

(20) Fanning, P. E.; Vannice, M.; Albert, A. DRIFTS study of the formation of surface groups on carbon by oxidation. *Carbon* **1993**, *31* (5), 721–730.

(21) Fuente, E.; Menéndez, J. A.; Díez, M. A.; Suárez, D.; Montes-Morán, M. A. Infrared spectroscopy of carbon materials: A quantum chemical study of model compounds. *J. Phys. Chem. B* **2003**, *107*, 6350–6359.

(22) Prest, W. M., Jr.; Mosher, R. A. Fourier transform IR spectroscopic characterization of the functional groups on carbon black. *ACS Symp. Ser.* **1982**, *200*, 225–247.

(23) Mawhinney, D. B.; Yates, J. T. FTIR study of the oxidation of amorphous carbon by ozone at 300K — direct COOH formation. *Carbon* **2001**, *39*, 1167–1173.

(24) Huang, C. D.; Xiong, Z. T.; Lin, J. Y.; Tan, K. L. Investigation of the electrochemical behavior of heat-treated carbon blacks and Pt/C catalysts. *Surf. Rev. Lett.* **2002**, *9* (3,4), 1443–1452.

(25) Lee, W. H.; Kim, J. Y.; Ko, Y. K.; Reucroft, P. J.; Zondlo, J. W. Surface analysis of carbon black waste materials from tire residues. *Appl. Surf. Sci.* **1999**, *141*, 107–113.

(26) Frejaville, C.; Karoui, H.; Tuccio, B.; Moigne, F. L.; Culcasi, M.; Pietri, S.; Lauricella, R.; Tordo, P. 5-(Diethoxyphosphoryl)-5-methyl-1-pyrroline N-oxide: A New Efficient Phosphorylated Nitrone for the in Vitro and in Vivo Spin Trapping of Oxygen-Centered Radicals. *J. Med. Chem.* **1995**, *38* (2), 258–265.

(27) Villamena, F.; Hadad, C. M.; Zweier, J. L. Kinetic Study and Theoretical Analysis of Hydroxyl Radical Trapping and Spin Adduct Decay of Alkoxycarbonyl and Dialkoxycarbonyl Nitrones in Aqueous Media. *J. Phys. Chem. A* **2003**, *107*, 4407–4414.

(28) Limbach, L. K.; Yuchun, L.; Grass, R. N.; Brunner, T. J.; Hintermann, M. A.; Gunther, D.; Stark, W. J. Oxide nanoparticle uptake in human lung fibroblasts: Effects of particle size, agglomeration and diffusion at low concentrations. *Environ. Sci. Technol.* **2005**, *39*, 9370–9376.

(29) Álvarez, P. M.; Masa, F. J.; Jaramillo, J.; Beltrán, F. J.; Gómez-Serrano, V. Kinetics of ozone decomposition on activated carbon. *Ind. Eng. Chem. Res.* **2008**, *47*, 2545–2553.

(30) Schröder, A.; Klüppel, M.; Schuster, R. H.; Heidberg, J. Surface energy distribution of carbon black measured by static gas adsorption. *Carbon* **2002**, *40*, 207–210.

(31) Chugtai, A. R.; Atteya, M. M. O.; Kim, J.; Konowalchuk, B. K.; Smith, D. M. Adsorption and adsorbate interaction at soot particle surfaces. *Carbon* **1998**, *36*, 1573–1589.

(32) Alam, M. S.; Camredon, M.; Rickard, A. R.; Carr, T.; Wyche, K. P.; Hornsby, K. E.; Monks, P. S.; Bloss, W. J. Total radical yields from tropospheric ethane ozonolysis. *Phys. Chem. Chem. Phys.* **2011**, *13*, 11002–11015.

(33) Mysak, E. R.; Smith, J. D.; Ashby, P. D.; Newberg, J. T.; Wilson, K. R.; Bluhm, H. Competitive reaction pathways for functionalization and volatilization in the heterogeneous oxidation of coronene thin films by hydroxyl radical and ozone. *Phys. Chem. Chem. Phys.* **2011**, *13*, 7554–7564.

(34) Donaldson, K.; Brown, D.; Clouter, A.; Duffin, R.; MacNee, W.; Renwick, L.; Tran, L.; Stone, V. The pulmonary toxicology of ultrafine particles. *J. Aerosol Med.* **2002**, *15*, 213–220.

(35) Dellinger, B.; Pryor, W. A.; Cueto, R.; Squadrito, G. L.; Hegde, V.; Deutsch, W. A. Role of free radicals in the toxicity of airborne fine particulate matter. *Chem. Res. Toxicol.* **2001**, *14*, 1371–1377.

(36) Khachatryan, L.; Vejerano, E.; Lomnicki, S.; Dellinger, B. *Environ. Sci. Technol.* **2011**, *45*, 8559–8566.